

pubs.acs.org/cm Article

Discovery of Dramatically Improved Ammonia Synthesis Catalysts through Hierarchical High-Throughput Catalyst Screening of the Fe(211) Surface

Jon Fuller, Alessandro Fortunelli,* William A. Goddard, III,* and Qi An*



Cite This: Chem. Mater. 2020, 32, 9914-9924



Read Online

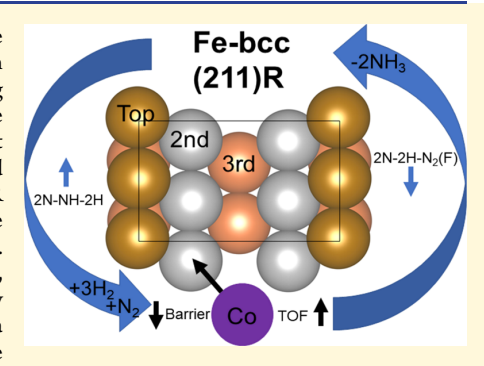
ACCESS

Metrics & More



Supporting Information

ABSTRACT: In order to improve efficiency of ammonia synthesis using the Haber–Bosch (HB) process with Fe-based catalysts, we employed quantum mechanics (QM)-based hierarchical high-throughput catalyst screening (HHTCS) of 49 possible metal dopants. Here, we consider the Fe(211) surface (one of the two most active iron catalyst facets) to identify dopants that dramatically increase the turnover frequency (TOF) for HB synthesis. We found that under HB conditions, this surface reconstructs to form the Fe(211)R missing-row surface. Focusing on dopants with a strong preference for the subsurface site, we found that Co is the most promising candidate among the 49. We then examined the full reaction pathway on this Co-doped Fe(211)R surface, considering all 19 important 2 × 2 configurations and calculated the free-energy barriers (ΔG^f) for all 12 important reaction steps. At 673 K and 20 atm, we find a decrease, $\delta(\Delta G^f) = -0.19$ eV, in the overall reaction free-energy barrier for the



Co-doped case. We then carried out kinetic Monte Carlo simulations for 60-120 min using 100 replicas with the full reaction path using rates from QM free-energy reaction barriers to predict that the TOF for the Co-doped surface increases by a factor of 2.8 with respect to the undoped Fe(211)R surface. Thus, the Co-doped Fe(211)R system could lower the extreme HB pressure of 200 atm to \sim 40 atm at 773 K while maintaining the same TOF as that of undoped Fe(211)R. We conclude that Co dopants in the Fe catalyst could significantly improve the catalytic efficiency of ammonia synthesis under industrial conditions. This excellent performance of the Co-doped system is explained in terms of a surface spin analysis on the N_2 -bonded configurations that show how Co dopants shift the N_2 surface-binding mode. This demonstrates that metal surface spins can be used as quantitative descriptors to understand reaction energetics. This study demonstrates that the HHTCS kinetic analysis of the free-energy reaction path in terms of essential configurations can enable discovery of the salient barriers to overcome and best dopant candidates for further improvements.

1. INTRODUCTION

The Haber–Bosch (HB) process of ammonia synthesis from nitrogen (N_2) and hydrogen (H_2) gases is a most important industrial chemical synthesis process, primarily for producing nitrate-based fertilizers. The HB process is the primary method of NH₃ production, with over 150 million tons per year of NH₃ produced for fertilizer manufacturing. The HB process requires elevated operating temperatures (typically 673–773 K) and pressures (50–200 atm) to produce suitable reaction rates for NH₃ synthesis. These conditions require significant capital investments and energy usage, making improving the efficiency of ammonia synthesis a very important challenge to achieve energy sustainability.

The typical industrial catalyst for HB synthesis of NH₃ is Febased, leading to 70% or higher efficiency for the HB process. Until the 1980s, the reaction pathway for the production of NH₃ on the catalytically active Fe surface orientations was very uncertain, but the Somorjai⁸ and Ertl⁷ groups provided qualitative insight, confirmed by further experimental⁹ and theoretical work. Particularly, Somorjai and Materer⁸ showed

that Fe-bcc(111) and Fe-bcc(211) single-crystal surfaces are significantly more active in NH $_3$ synthesis than Fe-bcc(100) and Fe-bcc(110). They interpreted this was due to second- and third-layer access to specific bonding sites (C7) available on these surfaces. Indeed, Fe-bcc(111) and Fe-bcc(211) were suggested as the most active surfaces for NH $_3$ synthesis under industrial conditions. L1,12 Extensive studies were reported for Fe-bcc(111), which led to TOF = 9.7/s per 2 × 2 site for 400 °C with H $_2$, N $_2$, and NH $_3$ pressures of 15:5:0.002 atm. The studies on Fe-bcc(211) were less complete (NH $_3$ pressure mot specified) but a TOF = 7.3/s per 2 × 2 site at 400 °C was reported. However, these experiments provided little detail on

Received: June 26, 2020 Revised: October 28, 2020 Published: November 17, 2020





the reaction mechanism and did not provide an adequate basis for developing improved catalysts.

Recently, we reported the first full reaction mechanism and kinetics on Fe-based catalysts. Using a 2 \times 2 periodic cell (6 layers thick), we applied the PBE-D3 flavor of density functional theory (DFT) to find that at 400 °C and 20 atm pressure, Febcc(111) has 24 important 2 \times 2 surface configurations and 12 important reaction steps. We used the predicted free-energy reaction barriers and reaction energies to carry out kinetic Monte Carlo (kMC) simulations for 60 min, leading to a predicted TOF = 17.7/s for H₂, N₂, and NH₃ pressures of 15:5:0.002 atm, in excellent agreement with TOF = 9.7/s experimental. These experiments on single-crystal Fe surfaces were most valuable in providing the basis for validating the accuracy of the QM calculations.

For the Fe-bcc(211) surface, we predicted that at 673 K and 20 atm of hydrogen and nitrogen, the Fe-(211)R missing-row type surface reconstruction is stabilized. Our kMC calculations lead to HB catalytic rates of 100:106 for Fe-bcc(111)/Fe-bcc(211)R in excellent agreement with an experimental ratio of 100:75. 11,12 Somorjai concluded that fourfold bonding sites are important for the NH $_3$ synthesis reaction. 8 Our simulations indicate that the Fe-bcc(211)R surface adopts a terraced configuration because of the missing-row reconstruction, therefore exposing additional "deep" sites. These fourfold sites were found to be involved in the N $_2$ dissociation process in our previous work, which determined the primary reaction barriers on the Fe(211)R surface. 12

Electrochemical techniques¹³ have promise for NH₃ synthesis. This would provide lower temperatures and pressures while obtaining the H for NH3 synthesis from water rather than H₂ from water-gas shift, which would considerably decrease the energy consumption while reducing the enormous CO2 produced by water-gas shift. 14,15 However, efficient electrocatalysts for N2 reduction have not yet been developed. Similarly, photoelectrocatalysts¹⁶ that can produce ammonia using Mg-based catalysts to synthesize NH3 using natural gas, water, and atmospheric N2 are currently being researched but also have not reached the industrial scale and levels of sustainability necessary for current NH₃ demands. 17 It has been shown that ruthenium-based catalysts might lead to more efficient HB catalysis than iron-based catalysts, 18 but both environmental and economic reasons have impeded use of Ru in commercial applications.

Herein, we focus on how to improve the catalytic activity of the industrially relevant Fe-bcc(211)R surface by doping it with various metal species in order to lower the overall reaction barriers. Here, we start from the free-energy reaction diagram including 19 important intermediates and 12 important reaction steps for the Fe-bcc(211)R NH₃ synthesis pathway that we studied previously using a 2 × 2 surface configuration ¹² at both 400 and 500 °C (bounds for industrial conditions in HB). We focus on pressures used in Somorjai's foundational work (H₂/N₂/NH₃ = 15/5/1 atm)⁸ and those currently used in the industry (e.g., $H_2/N_2/NH_3 \sim 150/50/1$ atm).

Because the computational requirements for determining the free energies of equilibrium configurations and transition states for the entire reaction pathway for doped catalysts are intense, we employ our hierarchical high-throughput catalyst screening (HHTCS) strategy used in our previous studies for doping the Fe-bcc(111) surface. The HHTCS approach allows a rapid screening of catalyst modifications (e.g., addition of metal dopants) by determining its effect on important states directly

related to the primary reaction barriers on the Fe-bcc(211)R surface. This approach allows us to focus on the most promising few in decreasing the reaction energy barriers to improve the reaction rates. This allows us to dramatically accelerate in silico predictions for the 49 dopants, narrowing the possibilities to a few most promising ones that we can examine more completely for accurate kinetics. ^{19–21} We previously applied HHTCS to HB synthesis on the Fe-bcc(111) surface where we successfully identified several effective dopants, Ni, Si, Rh, Pt, Cu, and Pd. ^{19–21} In particular, we found that Si-doped Fe-bcc(111) can reduce the severe HB industrial (200 atm/500 °C) conditions to much milder conditions (60 atm/400 °C) while maintaining a similar TOF. ²¹

For all 49 elemental dopants, we applied the HHTCS criteria sequentially, based on the important reaction barriers for the pure Fe-bcc(211)R surface. This eliminated 46 dopants, leaving just 3 good dopant candidates (i.e., Co, Ru, and Zr) that could potentially reduce the overall free-energy barrier for NH₃ synthesis. The predicted performance for these three good candidates compared to pure Fe was ~26 times for Co, ~3.5 times for Zr, and ~3 times for Ru using transition state theory (TST) and the primary barrier found from QM. 11

Then, for the Co-doped Fe-bcc(211)R surface, we examined the complete free-energy reaction diagram including all 19 intermediate states and 12 transition states important to the synthesis reaction, using the same computational setup as on the pure Fe-bcc(211)R surface. Based on the QM free-energy barriers, we employed kMC calculation using 100 replicas and 60 min to predict reaction rates for NH₃ production under various pressure and temperature conditions. Assuming stoichiometric conditions, we find that the TOF for the Co-doped system is 2.8–4.0 higher than the pure Fe system. We also examined how the rates would change under nonstoichiometric conditions, under which we find that at 500 C and $\rm H_2/N_2/NH_3$ = 30:10:1 atm, the TOF is 642 NH₃/s/(2 × 2) for the doped surface, which is comparable to the pure Fe system at much higher total pressure (200 atm) and the same temperature.

Thus, for the Co-doped surface, the TOF increases by a factor of ~threefold to ~sevenfold depending on reaction conditions compared to the pure Fe surface. Reduction of the total pressure from 200 to 40 atm at 773 K leads to a TOF within 5% of pure Fe(211)R at 200 atm. This suggests that Co doping could improve significantly the catalytic efficiency of Fe catalysts in ammonia synthesis under industrial conditions. We also rationalized why Co improved the catalytic performance using a valence-bond analysis of Co's effect on the chemical bonding in the most important surface configurations.

2. COMPUTATIONAL METHODS

2.1. QM Predictions. The full free-energy pathway for Febcc(211)R free-energy synthesis obtained in our previous work was used as the basis for all calculations. These results were obtained using the Vienna Ab-Initio Simulation Package (VASP)^{22–24} to perform DFT calculations to obtain the electronic energy and phonon corrections obtained from phonon vibration calculations using the harmonic approximation to calculate the free energy of each state in the synthesis pathway. All calculations were performed using the Perdew–Burke–Ernzerhoff (PBE)^{25,26} functional with D3 empirical corrections (PBE-D3) for van der Waals interactions.²⁷

We used a self-consistent field electronic energy convergence threshold of 10^{-6} eV for all calculations, consistent with our previous work. The unit cell was chosen to be a (2×2) configuration with a k-point sampling of $4 \times 4 \times 1$ for the x y z directions; the z direction was

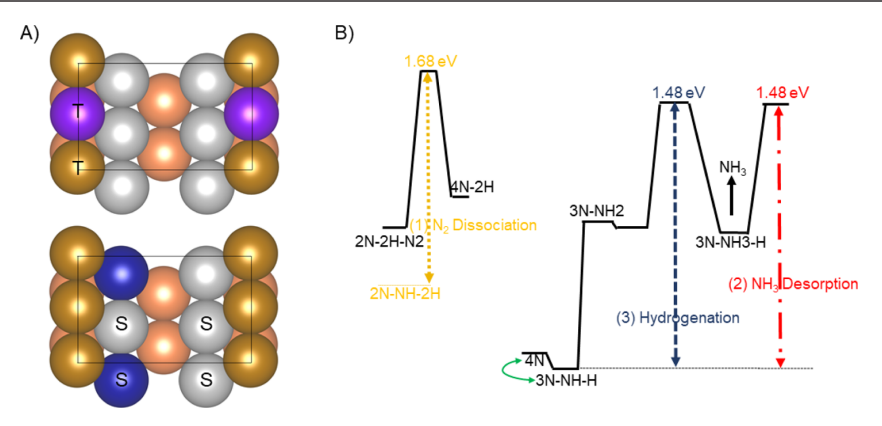


Figure 1. (A) Fe-bcc(211)R surface of the (2×2) unit cell with one substitutional top-layer atom (shown in purple in the top image) or one substitutional second-layer atom (shown in blue in the bottom image). The surface shows the first three layers of Fe atoms on Fe-bcc(211)R represented by bronze (top), silver (second), and orange (third) spheres. Alternative doping sites for the top and second layer are also marked with T (top) or S (second). (B) Simplified Fe(211)R standard-state free-energy diagram obtained from DFT/PBE-D3 calculation for NH₃ synthesis at T = 673 K, $P(H_2) = 15$ atm, $P(N_2) = 5$ atm, and $P(NH_3) = 1$ atm. All three barriers important in the HHTCS method are shown in color and numbered, with barrier 1 (N_2 dissociation) shown on the left, barrier 2 (NH_3 desorption) and barrier 3 (hydrogenation) shown on the right. 4N and 3N-NH-H are both plausible reference states for doped systems as these two states can both be the lowest energy state depending on the specific surface (or subsurface) dopants.

chosen to include a layer of vacuum (\sim 15 Å) in order to minimize interactions with periodic images.

We used the nudged elastic band²⁸ method (combined with dimer calculations²⁹ for ambiguous cases) to find true transition states with a single negative frequency in the Hessian matrix. The free-energy corrections and zero-point energy for gas phases were taken from previous simulations.¹² Optimized per-atom magnetic moments are computed for Fe and other magnetic dopant elements for all calculations. The magnetic moments of magnetic elements are initialized with values near the normal magnetic moments of the bulk metals. The nonmagnetic species have moments of 0. A full explanation of the simulation configuration can be found in previous work.¹²

2.2. HHTCS Design and Selection Criteria. We considered 49 distinct elemental dopants for improving the efficiency of the Febcc(211)R catalytic surface. For each dopant, the complexity and number of simulations required to fully evaluate the NH3 synthesis pathways for any given candidate are enormous, making it impractical to apply to 49 dopants. We showed previously 19,20 that HHTCS drastically reduces the computational requirements in the search for new and more efficient catalysts. Using the HHTCS method with properly designed criteria, the pool of 49 elemental species was considerably narrowed leaving only 3 candidate dopants. These criteria were based on the important reaction barriers from NH3 synthesis on pure Fe-bcc(211)R from previous work, focusing on target conditions for an improved HB process of T = 673 K and 20 atm total reactant pressure. These barriers were estimated on the pool of candidate elements via two simple ionic relaxation calculations to obtain the electronic energy for the positions for each criterion, then obtaining an estimated free-energy barrier by adding phonon corrections taken from the pure Fe-bcc(211)R surface.

Because of the complexity of the reconstructed Fe(211) surface (Figure 1), several potential doping sites are available for each dopant. Therefore, the first step in our HHTCS was to determine the preferred surface or subsurface doping sites for each of the considered 49 elements. Each of the six positions was evaluated for each of the 49 initial species using the 4N state as shown in refs 11 and 12. In this state, two nitrogen atoms are adsorbed in the exposed trough region left open by the removed "missing-row" reconstruction of the Fe-bcc(211) surface^{30–32} and two additional nitrogen atoms are adsorbed in the second layer of the surface. This is roughly equivalent exposure to adsorbed nitrogen in each of the four distinct second-layer doping sites along with two distinct first-layer doping sites, making this state ideal for evaluating the preferred (lowest energy) doping location for each

element. Figure S1 of the Supporting Information shows the optimum doping sites for the 49 elements based on their lowest electronic energy position in the low-energy $4N^{**}$ state.

The primary energy barrier for NH₃ synthesis on the pure Fe(211)R surface corresponds to N₂ dissociation from $2N-2H-N_2(F)$ state to 4N-2H state, with 2N-NH-2H being the dynamical resting state. Therefore, an effective dopant must decrease this primary energy barrier. Thus, the free-energy difference ΔG between these 2N-NH-2H and $2N-2H-N_2(F)$ states was selected as the first criterion assuming that the dissociation barrier will scale accordingly, that is, assuming Brønsted–Evans–Polanyi relationships. Specifically, we assumed that the phonon vibrational spectrum does not change significantly with a dopant. All species were evaluated in their preferred position according to the first step in the corresponding positions for the 2N-NH-2H and $2N-2H-N_2(F)$ configurations. Because the pure Fe-bcc(211)R surface has $\Delta G^{\dagger} = 1.68$ eV for this primary energy barrier, any element found to have a $\Delta G^{\dagger} < 1.68$ eV was retained for the next step in the HHTCS protocol. This criterion is then written as

$$\Delta E\{2N - NH - 2H + N_2 + H_2$$

 $\rightarrow 2N - 2H - N_2(F) + NH_3\} + 1.599 \text{ eV}$
 $< 1.68 \text{ eV}$ (1)

where 2N-NH-2H and $2N-2H-N_2(F)$ are the discussed surface configurations, N_2 , H_2 , and NH_3 are gas-phase molecules, and " ΔE " refers to the electronic energy difference between the states after and before the reaction. The constant term 1.599 eV is the free-energy corrections for pure Fe.

Because of the importance of the NH_3 desorption barrier on Febcc(211)R, our second criterion was the free-energy difference between the secondary resting state, $3\mathrm{N-NH-H}$, and the state immediately prior to the NH_3 desorption, $3\mathrm{N-NH}_3$ —H. In order to account for the differences in the lowest-energy state due to doping species behavior, we evaluated some cases using $4\mathrm{N}$ as the low-energy state instead of $3\mathrm{N-NH-H}$. Thus, this criterion is written as

$$\Delta E\{3N - NH - H + H_2$$

 $\rightarrow 3N - NH_3 - H\} + 1.059 \text{ eV}$
 $< 1.68 \text{ eV}$ (2)

or in the case of species with a lower electronic energy 4N state than the $3N{-}NH{-}H$ state, as

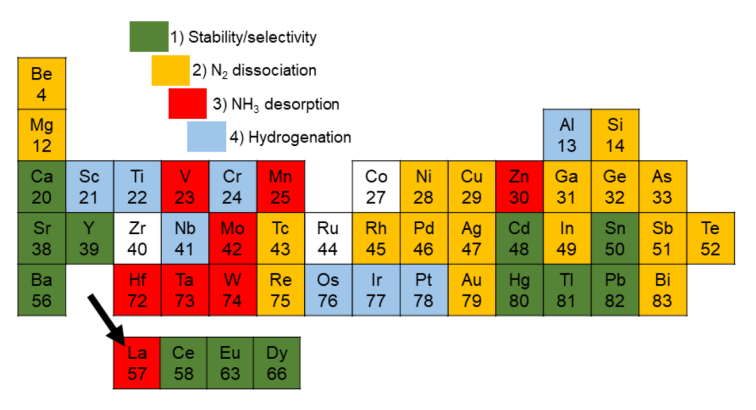


Figure 2. 49 elements selected for initial investigation using the HHTCS method, including Row 4, 5, and 6 transition metals along with alkaline earth metals and several metalloids and other metals. Radioactive elements were avoided for industrial considerations, as well as extremely rare or valuable metals. A small selection of lanthanides was tested additionally. Screening results for each element are shown via color shading, with elements in white passing all criteria. The arrow represented the selected lanthanide elements in HHTCS.

$$\Delta E\{4N + 2H_2 \rightarrow 3N - NH_3 - H\} + 2.976 \text{ eV} < 1.68 \text{ eV}$$
(3)

where the constant terms 1.059 eV and 2.976 represent the free-energy corrections for the pure Fe(211)R surface for 3N-NH-H and 4N secondary resting states, respectively.

The third criterion was aimed at ensuring that hydrogenation barriers were not greater than the main energy barrier for pure Febcc(211)R. Thus, we compare the preferred lowest-energy state (4N or 3N–NH–H, as determined by the previous criterion) with the 3N–NH $_2$ –2H state. The free-energy barrier of this hydrogenation step was estimated using two states 3N–NH $_2$ –2H and 3N–NH–H/4N, discarding cases exhibiting a ΔG^{\dagger} higher than the overall reaction barrier of 1.68 eV. This criterion is written in two ways, depending on whether 4N or 3N–NH–H is the low-energy state, as

$$\Delta E\{3N - NH - H + H_2$$

 $\rightarrow 3N - NH_2 - 2H\} + 1.595 \text{ eV}$
 $< 1.68 \text{ eV}$ (4)

$$\Delta E\{4N + 2H_2 \rightarrow 3N - NH_2 - 2H\} + 2.666 \text{ eV} < 1.68 \text{ eV}$$

where the constant terms 1.595 and 2.666 eV represent the free energy on pure Fe-bcc(211)R using 3N-NH-H and 4N as the resting state, respectively. All positions previously described in these criteria are shown in Section 3.2.

2.3. Surface Reconstruction and Hydrogen Poisoning. To further ensure the viability of the doped Fe(211)R surface with the most promising dopant from HHTCS, several additional calculations were performed in addition to the normal synthesis pathway states obtained previously. ¹² All potential resting states found in the original pathway (4N, 3N–NH–H, and 2N–NH–2H) were evaluated with dopants placed in each of the 4 second-layer doping sites to ensure that alternative doping configurations were not preferable to the state determined to be favorable for the dopant in the first step.

Additionally, the surface reconstruction energy 33,34 was checked for the 3 promising dopants using a bilayer surface energy calculation method for doped Fe-bcc(211) and Fe-bcc(211)R surfaces with both H and N adsorption under elevated temperatures to ensure that the reconstructed surface was still energetically preferable on the doped surface. The full details for this method can be found in our previous work. 12

Hydrogen poisoning was not considered in the HHTCS because it depends on hydrogen pressure, and the poisoning configurations may include 2N-2H and 2N-4N. The hydrogen poisoning was considered for the 3 most promising elements passing the HHTCS criteria using the 2N-4H configuration as the reference state.

- **2.4. Reaction Mechanism.** The HB reaction mechanisms on Fe surfaces, including hydrogenation, ³⁵ N₂ dissociation, and NH₃ desorption, were investigated extensively in our prior work on both Fe-bcc(111) and Fe-bcc(211)R surface orientations ^{11,12} as well as on the unreconstructed Fe-bcc(211) surface. ³⁶ Here, we determine the full synthesis reaction pathway on the pure Fe surface, ¹² for the best-performing dopant candidate singled out by the HHTCS search to obtain the full QM free-energy values using the methodology described in Section 2.1 and in previous work. ¹² Some streamlining of the reaction diagram was performed. Thus, the intermediate 4N structure was found to be not important, so we removed its accompanying transition state from the analysts. This leaves in 21 distinct equilibrium states and 23 transition states for the full reaction pathway.
- **2.5. kMC Simulations.** To fully exploit the detailed information from the QM free-energy diagram and transform it into accurate predictions of catalyst kinetics, we use the kMC approach.³⁷ We employ a mean-field kMC model³⁸ in which
 - (i) the nodes of the kMC network and their free energies are taken from the QM local minimum configurations of the (2 × 2) Febcc(211)R unit cell,
 - (ii) we use the QM saddle point free energies to estimate transition rates among kMC nodes via TST. That is, we take transition rate = $(k_{\rm B}T/h)\exp(-\Delta G^{\dagger}/k_{\rm B}T)$, where ΔG^{\dagger} is the difference in free energy between the initial and transition (saddle point) state,
 - (iii) we run cyclic kMC simulations using 100 independent replicas and 2 × 10⁹ kMC steps for each replica, corresponding to few to several hours of the real-time steady-state HB process, with results converged within ~2% accuracy. As in our previous work, for Eley−Rideal (ER) steps involving gas-phase species turning into adsorbates, we calculate the rate of the backward (desorption) process via TST and exploit the microscopic reversibility principle (i.e., thermodynamic equilibrium) to calculate the forward ER rate. To this end, the free energy of the desorption transition state is evaluated as the sum of the final (adsorbed) state plus the electronic desorption energy (including zero-point energy corrections). These technical points are less important than on Fe-bcc(111) because the rate-determining steps on Fe-bcc(211)R are of Langmuir− Hinshelwood type and not ER.

3. RESULTS AND DISCUSSION

3.1. Hierarchical High-Throughput Catalyst Screening. All 49 elements (shown in Figure 2) were found to prefer a specific top- or second-layer doping position in the first step. Testing for preferred doping position included both the important position for final N_2 dissociation $(2N-2H-N_2(F))$

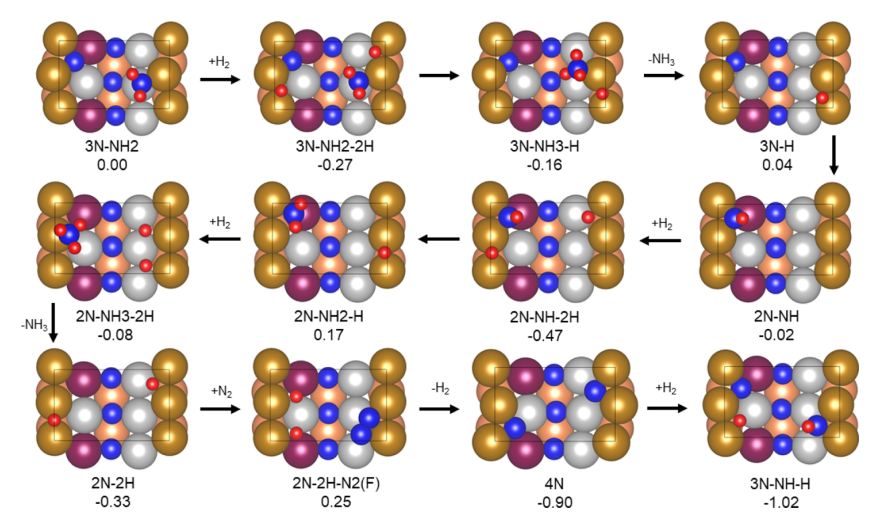


Figure 3. Full reaction pathway for NH_3 synthesis on the Co-doped Fe-bcc(211)R catalytic surface. Top-layer Fe atoms are illustrated with bronze spheres, while silver spheres and orange spheres indicate second- and third-layer Fe atoms. Nitrogen and hydrogen are shown as blue and red spheres, respectively; the doped Co atom is illustrated with a purple sphere in the second layer. The N_2 dissociation process along with details on all transition states are shown in Figure 4. Free energy ΔG (in eV) is shown for each state with reference to the ground state $3N-NH_2$.

Table 1. Comparison of Dopant Candidates Remaining at the Final Stage (Criterion-3) of HHTCS at T = 673 K and Pressure $H_2/N_2/NH_3 = 15:5:1$ atm^a

element	preferred resting state	barrier 1 (eV)	barrier 2 (eV)	barrier 3 (eV)	overall barrier (eV)	predicted rate (NH $_3/s$ for 2 × 2 unit cell)
Co	3N-NH-H	1.49	1.47	1.42	1.49	195
Zr	4N	1.59	1.41	1.61	1.61	25
Ru	4N	1.52	1.56	1.62	1.62	21
Pure Fe	3N-NH-H	1.68	1.48	1.48	1.68	7
Al	4N	1.44	1.60	1.70	1.70	
Cr	4N	1.44	1.61	1.81	1.81	
Os	3N-NH-H	1.49	1.24	1.91	1.91	
Nb	3N-NH-H	1.46	1.33	1.93	1.93	
Ir	4N	1.42	1.63	1.93	1.93	
Ti	3N-NH-H	1.21	1.55	1.95	1.95	
Pt	3N-NH-H	1.52	1.21	2.34	2.34	

[&]quot;Co was estimated to have the greatest improvement on the overall energy barrier for NH₃ synthesis on Fe-bcc(211)R and was selected for comprehensive testing of the full reaction pathway.

on the surface as well as the low-energy 4N state, both shown in Figure 3. Several elements (e.g., Ca, Cd, and Hg) were found to be unsuitable for the proposed reaction mechanism because of their effects on the surface relating to strong N-dopant binding and were eliminated in this initial stability check.

The results of this initial step are included in Table S1 of the Supporting Information. Based on their preferred position, they were then tested against criteria 1–3 to evaluate the dopant's effects on the overall energy barrier in the reaction pathway. Some elements, including lanthanides and larger transition metals and alkaline earth metals, were found to exhibit an unusual surface relaxation, as shown in Figure S2 of the Supporting Information. A total of 12 elements were found to exhibit this unusual relaxation that undermined the previously established reaction mechanism. Thus, they were not continued in HHTCS. This leaves 37 elements for HHTCS. Further work may find novel reaction mechanisms that suit these 12 other dopants better.

A total of 19 elements out of the 37 elements tested were found to improve the primary reaction energy barrier as a result of the first criterion and were selected to advance in HHTCS. A

total of 18 elements, including all of the metalloids and several Row 5 and Row 6 transition metals, were found to not improve the primary energy barrier and were discarded.

Unlike the first criterion, which utilizes 2N-NH-2H as the low-energy resting state for evaluating the primary barrier, the second criterion requires the lower-energy state from two very similar states in the full pathway, 4N and 3N-NH-H. In the pure Fe-bcc(211)R surface, 3N-NH-H is lower in energy and thus appropriate to evaluate overall barriers. However, for some candidate species, the 4N state was found to be lower in energy, as shown in Table S2 of the Supporting Information. Thus, we used two separate calculations to evaluate the third criterion as described in eqs 2 and 3 in section 2.2. From the second criterion, we find that 8 of the 19 species have an NH3 dissociation barrier that is higher than the overall energy barrier $(N_2 \text{ dissociation})$ for Fe-bcc(211)R, indicating that they are not suitable catalyst dopants. A selection of 11 elements were found to have ΔG^{\dagger} < 1.68 eV from this criterion, indicating suitability for further testing in the HHTCS method.

In the third criterion, the first hydrogenation step of the reaction and an important barrier to the synthesis reaction on

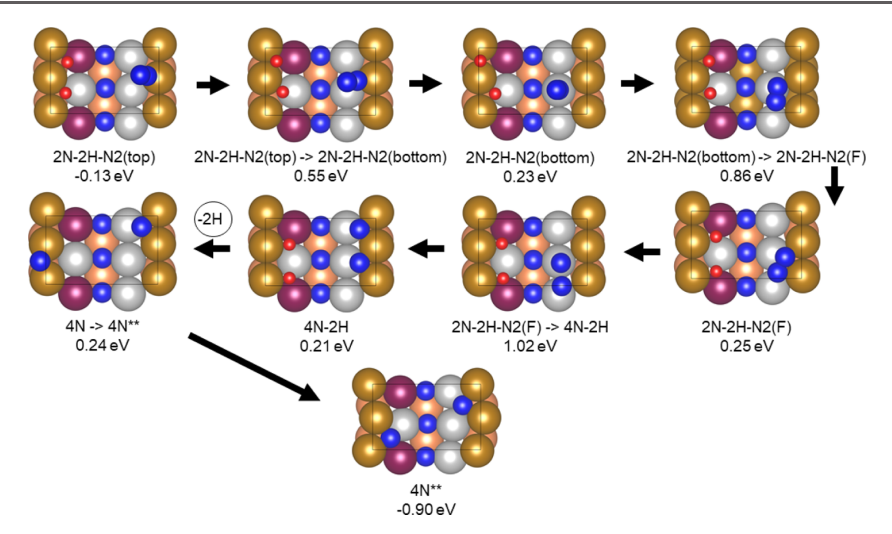


Figure 4. Detailed N_2 dissociation pathway on the Co-doped Fe(211)R surface. Transition states obtained from NEB/dimer calculations are shown for each important transition in the dissociation pathway. Free energy (ΔG) for each state is shown in eV.

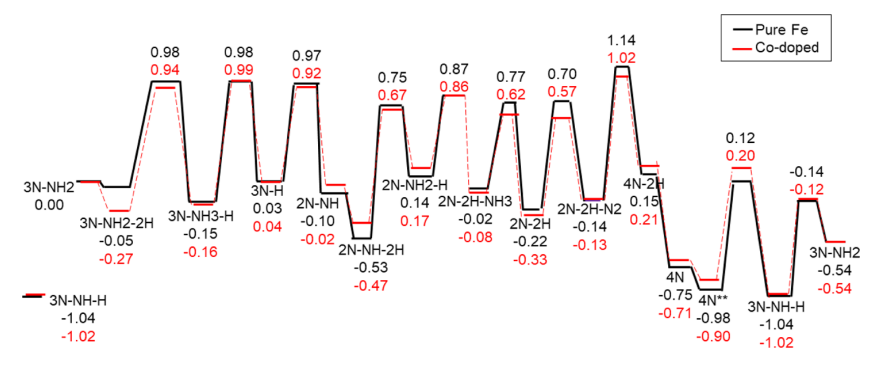


Figure 5. Standard free-energy diagram comparison between pure Fe-bcc(211)R (black) and Co-doped Fe-bcc(211)R (red). This free-energy diagram omits several states to preserve clarity; the complex N_2 dissociation pathway and 4N transitions are not shown. See Figures S3 and S4 for NEB details.

Fe-bcc(211)R, $3N-NH_2-2H \rightarrow 3N-NH_3-H$, were evaluated using the previously determined low-energy state (4N or 3N-NH-H, as described above) as described in eqs 4 and 5 in section 2.2. After this screening, only three dopant elements were found to improve the primary energy barrier across all criteria: Co, Ru, and Zr.

Ru-based catalysts have long been suggested as a possible alternative to the industrial Fe catalyst, with comprehensive computational work performed using similar DFT methods 40,41 for Ru nanoparticle catalysis as well as proposed methods to use more complex catalyst designs in combination with Ru for efficient ammonia synthesis.⁴² Additionally, ZrN has been of interest in ongoing metal nitride catalyst research for NH3 and has been investigated computationally as a potentially viable catalyst for electrochemical synthesis. 43 Of these three remaining elements in our work, we found Co to have the most significant reduction in energy barriers (as shown in Table 1 below). Co-based catalysts have been an increased focus of research in a variety of alternate synthesis mechanisms, such as associative (ER) NH₃ formation on the complex Co-N-C⁴⁴ and Co₃Mo₃N⁴⁵ catalysts in attempts to find lower-energy approaches to efficient NH3 synthesis. We thus selected Co as

the candidate for further evaluation in the NH_3 synthesis reaction on Fe-bcc(211)R.

Finally, we evaluated the preferred doping site using the 4N state in the first step of HHTCS. To make sure that the doping site is not changed in other plausible resting states, we computed the electronic energies for all possible subsurface sites in configurations 4N, 3N–NH–H, and 2N–NH–2H. All of these positions for each resting state were found to be extremely similar in electronic energy to the initially determined position from the first step of HHTCS, and Co was deemed suitable in this location. In regard to the missing-row reconstruction of the Fe-bcc(211) surface, we found that the Co-doped Fe-bcc(211)R surface was suitable for calculating the full free-energy pathway for NH₃ synthesis.

3.2. Pathway including Barriers. The full mechanistic pathway for Co-doped Fe-bcc(211)R is depicted in Figure 3 for the key states in the reaction mechanism, with the complex N_2 dissociation pathway shown in Figure 4. The corresponding free-energy diagram is shown in Figure 5. The detailed NEB calculations for hydrogenation steps and N_2 dissociation steps are displayed in Figures S3 and S4 of the Supporting Information. Additionally, the full mechanistic pathway for the pure Fe-bcc(211)R surface is shown in Figure S5 of the

Supporting Information for additional clarity. We find that the Co-doped surface has an overall free-energy barrier of ΔG^f = 1.49 eV (at T=673 K and $P(\mathrm{H_2})=15$ atm, $P(\mathrm{N_2})=5$ atm, $P(\mathrm{NH_3})=1$ atm) corresponding to the free-energy difference between the 2N–NH–2H dynamical resting state and the N₂ dissociation step. This was previously found to be the primary energy barrier on the pure Fe-bcc(211)R surface with $\Delta G^{\dagger}=1.68$ eV. Additionally, there is also a secondary, numerically very close free-energy barrier with $\Delta G^{\dagger}=1.47$ eV, corresponding to the free-energy difference between the 3N–NH–H secondary dynamical resting state and the NH₃ desorption step from 3N–NH–H. We will examine the main mechanistic steps and how they are affected by Co doping in more detail.

For N_2 dissociation (shown in Figure 4 above), the effect of the Co dopant is to make the 2N-NH-2H state slightly higher in energy ($\Delta G = -0.47$ eV compared to $\Delta G = -0.53$ for pure Fe) and especially to lower the free energy of the transition state for N_2 dissociation from 1.14 to 1.02 eV, both of which contribute to the decreased overall free-energy barrier. However, the dopant does not change significantly the energies of the 3N-NH-H state and the NH_3 desorption saddle point so that the doped system comes close to hitting the secondary barrier on pure Fe-bcc(211)R. The complex N_2 path prior to dissociation is qualitatively similar in both the Co-doped and pure surfaces with the N_2 molecule adsorbing on a first-layer site of the surface in a perpendicular mode prior to transitioning into a similar perpendicular position on a second-layer Fe atom, then shifting to a tilted "Final" position prior to dissociation in both

Interestingly, Figure 6 represented above shows that even though the adsorbed N_2 molecule lies on the opposite side of the

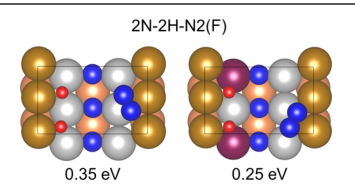


Figure 6. Comparison of the 2N-2H-N2(F) configuration for Febcc(211)R and Co-doped bcc(211)R. The N_2 molecule adopts an alternate tilted final position on the Co-doped surface. Details of the reasons behind this are found in Section 3.4. Free energies (ΔG) are included in eV below each position. The Co-doped state is found to be 0.10 eV lower than pure Fe-bcc(211)R, which contributes significantly to lowering the overall barrier for the reaction (N_2 dissociation).

Fe-bcc(211)R surface with respect to the Co doping location, Co still significantly lowers the energy of the 2N-2H-N2(F) configuration. This translates into lowering the energy of the resulting transition state for the N_2 dissociation. The decrease in the overall energy barrier for the Fe-bcc(211)R surface with Co doping by 0.19 eV is expected to significantly increase reaction rates, as we will see in the next section.

The secondary barrier at T=673 K corresponds to desorption of NH $_3$ from the surface (3N–NH $_3$ –H \rightarrow 3N–H) with respect to the 3N–NH–H secondary dynamical resting state, which has a $\Delta G^{\dagger}=1.47$ eV. The free energy of the NH $_3$ desorption transition state here is slightly higher than on the pure Fe(211)R surface: $\Delta G=0.99$ eV versus $\Delta G=0.98$ eV with respect to the reference state 3N–NH $_2$. However, the 3N–NH–H state has $\Delta G=-1.02$ eV in the Co-doped surface versus $\Delta G=-1.04$ eV in the pure Fe surface so that the overall energy barrier is slightly lower in the Co-doped surface ($\Delta G^{\dagger}=1.47$ eV compared to $\Delta G^{\dagger}=1.48$ eV for pure Fe).

The tertiary barrier for the reaction on both surfaces at T=673 K is the hydrogenation step $(3N-NH_2-2H$ to $3N-NH_3-H)$, involved in the formation of the NH_3 molecule. For the Codoped surface, this has $\Delta G^{\dagger}=1.42$ eV, while in the pure Fe surface, $\Delta G^{\dagger}=1.48$ eV.

Hydrogen poisoning was investigated as on the Fe-bcc(211)R surface 12 by comparing the free energies for the 2N-2H state (prior to N_2 molecule adsorption onto the surface) and the 2N-4H state with two additional H atoms adsorbed to the surface, which would poison the surface. At 673 K, as in pure Febcc(211)R, the 2N-4H state does not become a resting state, so this type of poisoning is not effective. At 773 K, however, this hydrogen poisoning plays a role in pure Fe-bcc(211)R but not on Co-doped pure Fe(211)R because the 2N-4H state lies 0.12 eV above the 2N-2H state.

In the un-reconstructed Fe-bcc(211) surface, C7 sites are believed to be important for the NH₃ synthesis reaction as noted by Somorjai and Materer.⁸ For Fe-bcc(211)R, our previous research indicated that the removal of the central row of atoms removes the C7 coordination but exposes additional fourfold binding sites between the second- and first-layer Fe atoms for N and NH_x species on the surface.¹² This facilitates several important processes along the reaction pathway, including N₂ dissociation and the restoration to the 4N** state before the synthesis cycle begins anew. For the N₂ dissociation process, each N atom is separated into fourfold sites on the same side of the trough region on the surface, while in the 4N** position, the

Table 2. Reaction Rates and Percent Populations P_i (i.e., Residence Times) = t_i (%) for the Most Relevant Configurations in (2 × 2) Unit Cells of Pure and Co-Doped Fe(211)R Surfaces under Steady State of Ammonia Synthesis as Predicted by kMC Simulations under Different Conditions. H_{2^j} N_{2^j} and NH_3 Pressures in atm. $P(NH_3) = 1$ atm in All Cases

	T = 673 K $P(H_2, N_2, NH_3) = (15,5,1)$ Fe(211)R	T = 673 K $P(H_2N_2NH_3) = (15,5,1)$ Co-Fe(211)R	T = 773 K $P(H_2, N_2, NH_3) = (150, 50, 1)$ Fe(211)R	T = 773 K $P(H_2, N_2, NH_3) = (150,50,1)$ Co-Fe(211)R	T = 773 K $P(H_2N_2NH_3) = (30,10,1)$ Co-Fe(211)R
Configuration	$P_i = t_i$ (%)	$P_i = t_i$ (%)	$P_i = t_i \ (\%)$	$P_i = t_i \ (\%)$	$P_i = t_i \ (\%)$
$3N-NH_2-2H$	7.60×10^{-4}	0.39	1.21×10^{-3}	3.04	0.74
2N-NH-2H	48.11	6.45	4.16	5.28	2.74
2N-2H	0.23	0.52	6.60	16.92	20.43
$2N-2H-N_2(top)$	5.67×10^{-2}	1.64×10^{-2}	1.15	0.65	0.16
4N	11.88	10.26	14.02	2.76	16.64
3N-NH-H	33.42	81.19	17.13	43.07	52.17
2N-4H	5.96	0.73	56.83	27.92	6.74
predicted TOF NH ₃ mol/s/ (2×2)	3.85	10.9	682	2691	649

Chemistry of Materials Article pubs.acs.org/cm

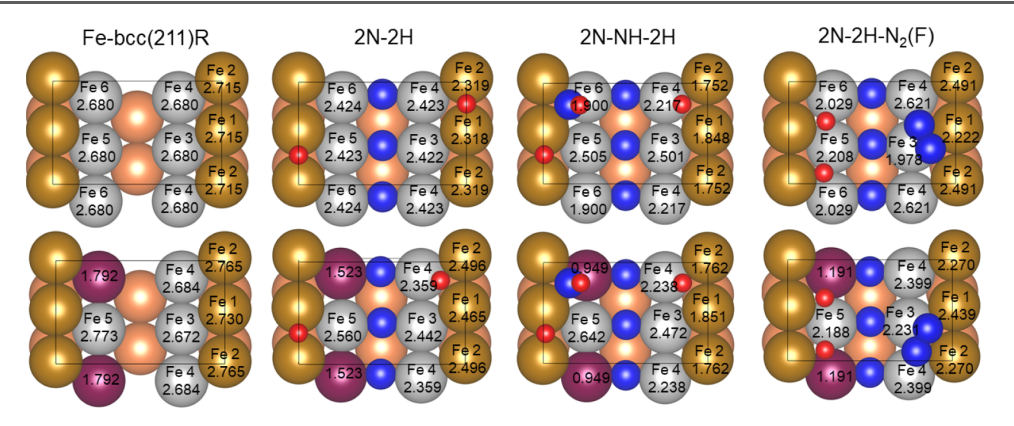


Figure 7. Magnetization of top- and second-layer Fe atoms in the blank Fe-bcc(211)R, 2N-2H, 2N-NH-2H, and 2N-2H-N₂(F) states (top) and Co-doped Fe-bcc(211)R for the same states (bottom). Fe positions 1–6 in the pure Fe case (1–5 on the Co-doped surface, with the doped Co atom replacing the 6th Fe atom) are labeled for clarity of discussion. Co is found to increase overall spin in the 2N-NH-2H case, resulting in a higher electronic energy for this position relative to the pure Fe surface, while differences in bonding are found in the 2N-NH-2H(F) position in the presence of Co on the surface resulting in lower energy for this position. Magnetization values are given in μB .

N atoms reach their lowest-energy configuration deeply bonded in fourfold sites after migration to opposite sides of the trough region. These positions are shown in Figure 4.

- 3.3. kMC Rates and Comparison to Prior Research on 211 Pure Fe. To determine the effect of Co doping on NH₃ production rates, we focus for simplicity on two sets of reaction conditions:
 - (a) HB: $P(H_2) = 150$ atm, $P(N_2) = 50$ atm, $P(N_3) = 1$ atm, and T = 773 K, which is similar to the operating conditions of the current industrial HB process and
 - (b) Somorjai: $P(H_2) = 15$ atm, $P(N_2) = 5$ atm, $P(N_3) = 1$ atm, and T = 673 K, which was used in Somorjai's singlecrystal experiments and which are target conditions for an HB process with a drastically decreased energy consumption.

Decreasing the operating pressure is important to decrease capital costs and energy consumption because of the high cost of operating high-pressure plants. For these 2 sets of conditions, we predicted catalytic rates on both pure and Co-doped Febcc(211)R. As described in Section 3.2, we derive the freeenergy reaction barriers and transition probabilities for the kMC analysis from the QM data. For pure Fe-bcc(211)R, this is in Figure 2 of Fuller et al. 12 and for Co-doped Fe-bcc(211)R, it is in Figure 6, as mentioned above.

We run kMC simulations until kinetic rates are converged to within few percent, which correspond to from 1 to 10 h of steady-state HB catalysis.

To achieve an unbiased comparison, we use exactly the corresponding states and identical numerical parameters for the pure and Co-doped catalyst: 21 equilibrium states and 23 transition states, slightly reduced from the set of 24 states used previously. 12 The kMC results are summarized in Table 2, where we report the TOF together with percent populations (i.e., percent residence times) of all configurations with populations >1% under 3 operating conditions:

- (a) Somorjai: $P(H_2) = 15$ atm, $P(N_2) = 5$ atm, $P(N_3) = 1$ atm, and T = 673;
- (b) HB: $P(H_2) = 150$ atm, $P(N_2) = 50$ atm, $P(NH_3) = 1$ atm, and T = 773 K; and
- (c) Reduced pressure HB: $P(H_2) = 30$ atm, $P(N_2) = 10$ atm, $P(NH_3) = 1$ atm, and T = 773 K,

Here, (a, b) are given for both pure and Co-doped systems, whereas (c) is given only for Co-doped (211)R. These results confirm our expectation from HHTCS: doping the Febcc(211)R surface with Co in its optimally preferred doping site increases HB reaction rates significantly.

- (a) Somorjai: The increase is \sim threefold, from TOF = 3.85 $NH_3/s/(2 \times 2)$ on pure Fe to TOF = 10.9 $NH_3/s/(2 \times 2)$ on the doped surface
- (b) HB: TOF = 682 NH₃/s/(2 × 2) for Fe to TOF = 2691 $NH_3/s/(2 \times 2)$ for the Co-doped surface
- (c) Reduced pressure HB, 40 atm: TOF = 649 for Co-doped, nearly the same as for 200 atm on pure Fe.

The populations reported in Table 2 are consistent with our previous analysis of dynamical resting and transition states for Fe-bcc(211)R: for the Co-doped system at 673 K, the main dynamical resting state switches from 2N-NH-2H for pure Febcc(211)R to 3N-NH-H and at 773 K, the change is from 2N-4H to a mixture of 3N-NH-H and 2N-4H. The convergence with respect to the number of kMC steps for Febcc(211)R and Co-doped bcc(211)R is given at T = 673 K in Table S3 of the Supporting Information. For 40 atm, conditions (c), hydrogen poisoning is reduced because the population of 2N-4H is reduced so that the population of the two dynamical resting states 3N-NH-H and 2N-2H is more balanced. Thus, the system is approaching an ideal catalyst in which all main freeenergy barriers are the same.

3.4. Chemical Insights into the Co-Doped Fe(211)R Surface: Spin Analysis. Analysis and understanding of binding of adsorbates to transition-metal surfaces in terms of simple descriptors represent a challenge because of the complicated interplay of interactions between delocalized conduction orbitals and localized d-shell orbitals with adsorbate chemical species. To understand the origin of rate enhancement due to Co doping, we use here a valence-bond approach that correlates changes in the net spins on the metal atoms with the strength of metal/adsorbate bonding. This enables a simple rationalization of kinetic data as discussed here.

The spin values of the top- and second-layer Fe atoms and the second-layer Co dopant were analyzed as in our prior work to extract information on the chemical bonding in these systems and the changes induced by the dopant. 12,19 We focus on the

2N–2H, 2N–NH–2H, and 2N–2H–N₂(F) states as the key resting states and the primary state for the N₂ dissociation process, with the blank surface and 2N–2H state (because of its similarity to both the primary resting and high-energy states) used as a reference state for the spin analysis. Figure 7 illustrates the magnetizations for these four states in μ B. In the following discussion, Fe 1 and 2 refer to the first-layer Fe atoms, while Fe 3–6 refer to the second-layer Fe atoms for the pure Fe surface. For the Co-doped surface, the Co is the second layer. The spin values for Fe 2, 4, and 6 and the doping Co are shown repeatedly in the relevant periodic positions in Figure 7.

For the 2N-2H state, the first-layer Fe atoms in Febcc(211)R maintain nearly equal magnetization. Similarly, Fe 3-6 have nearly equal magnetization. This indicates relatively equal spin distribution across the pure Fe surface with a slight decrease in the first-layer atoms because of the H bonding in surface bridge sites.

The Co-doped Fe-bcc(211)R surface behaves slightly differently. The H atoms cause a shift into the offset site adjacent to Fe 4 from its prior bridge position between Fe 1 and Fe 2. This decreases the spin by 0.07 μB for Fe 4, indicating a weak interaction with this Fe atom. A corresponding increase of 0.147 μB for Fe 1 and 0.177 μB for Fe 2 is noted between the Codoped and Fe-bcc(211)R positions, indicating that the bridgetype bonding between two first-layer Fe atoms has shifted to a similar bonding position on the Co-doped surface between Fe 4 and Fe 1, with a relatively weak bond to the surface characteristic of all Fe positions on the (211)R surface. This shift is caused by the Co-doped surface. The presence of the Co atom alters the magnetization of both the adjacent Fe 5 (with an increase of $\sim 0.137 \,\mu\text{B}$ due to Co) and the ridge atoms Fe 1 and 2, causing the surface to prefer the offset H position found in more complex positions such as 2N-4H and 2N-NH-2H (shown in Figure

Using 2N-2H as a baseline, we compare it with the resting state 2N-NH-2H that establishes the barrier for N₂ dissociation, the primary barrier along the reaction pathway. 2N-NH-2H is found to prefer a nearly identical state to the undoped surface, with the NH molecule preferring a pocket site on the third layer similar to N-adatom binding, and the two H atoms preferring a bridge and offset site. In comparison with 2N-2H, Fe 6, Fe 1, and Fe 2 exhibit a spin decrease of \sim 0.52, \sim 0.47, and 0.57 μ B, respectively, because of the presence of the adsorbed NH molecule adjacent to it in Fe-bcc(211)R. This suggests the formation of two π -bonds of the NH molecule with surface Fe. For the Co-doped system, the Fe 6 corresponding to the Co atom exhibits a spin decrease of \sim 0.57 μ B from 2N–2H because of the tight binding of NH adjacent to the Co position on the surface. The right side of the trough region (Fe 1-4) is largely similar for Fe-bcc(211)R and Co-doped Fe-bcc(211)R, with a generally neutral spin change between 2N-2H and 2N-NH–2H. However, the Fe 5 magnetization differs by 0.137 μB between Fe-bcc(211)R and the doped surface, which leads to a significant overall spin increase for the system. This higher spin corresponds to less overall bonding, which directly leads to a higher energy. This rationalizes our finding that 2N-NH-2H in Co-doped Fe-bcc(211)R is 0.06 eV higher in energy than in Febcc(211)R (see Figure 4). This energy increase in the resting state directly influences the lowered primary barrier for the Codoped surface.

 $2N-2H-N_2(F)$ presents a somewhat more complex picture. The N_2 molecule in Fe(211)R is adsorbed in a tilted position above Fe 3 in the Fe(211)R surface, with two H atoms adsorbed

in pocket sites on the left side of the trough region (Fe 5 and 6). Interestingly, the alternate tilt position is found to be energetically favorable for the Co-doped surface, with the N2 molecule oriented in a similar tilted manner between Fe 3 and Fe 4. For both surfaces, we see a net spin decrease in the left side from 2N-2H due to H binding in the second layer in the displaced positions. It is important to note that H binds more strongly to the pocket site as N_2 appears in $2N-2H-N_2$ compared to the bridge site in 2N-NH-2H or 2N-2H. This is shown by the stronger decrease in spin indicating more bonding on Fe 5 and 6 and for the Fe-bcc(211)R in the corresponding cases relative to the effects on Fe 4 seen in 2N-NH-2H compared to 2N-2H. Because of the complexity of these states and the different tilt orientation of the adsorbed N₂ molecule, a simple overall spin comparison is not sufficient to explain the energetic behavior of the surface here.

Instead, we must investigate the individual Fe atoms involved in N₂ binding. Fe 3 plays an important role in both positions. For Fe-bcc(211)R, we find that the N₂ molecule is involved primarily in bonding with Fe 3 and Fe 1 (see Figure 5). In the Co-doped Fe(211)R position, the molecule has weaker bonding than Fe(211)R but across all four Fe atoms (Fe 1-4) on the right side instead of only the central Fe 1 and 3. This is shown by an increase of $\sim 0.21 \ \mu B$ on Fe 1 and $\sim 0.26 \ \mu B$ on Fe 3 with a corresponding decrease of \sim 0.22 μ B on Fe 2 and \sim 0.22 μ B for Fe 4 between the Fe-bcc(211)R and Co-doped Fe-bcc(211)R positions. Although the overall spin is similar between Febcc(211)R and Co-doped system, there is a change in bonding on the surface. Here, the π -bond found for Fe-bcc(211)R to be bonded strongly to Fe 3 is weakened for the alloy, while σ -bonds are found to be more strongly bonded to the Co-doped surface. This behavior is also apparent in the changes in bond distances between N₂ and the adjacent Fe atoms for the Fe-bcc(211)R and Co-doped Fe-bcc(211)R 2N-2H-N₂(F) positions, with the weakened π -bond on Fe 3 lengthening by \sim 0.15 A and strengthened σ -bond resulting in a bond distance decrease of \sim 0.23 A between the N₂ molecule and Fe 4. The increased bond strength between N_2 and Co-doped Fe-bcc(211)R decisively contributes to the lower overall energy barrier for the reaction.

Our predictions on metal spin distribution and changes upon doping are in principle amenable to experimental validation via Mössbauer measurements on Fe single crystals. Our previous findings on N_2 bonding transformations from σ bond to π bond on the Fe-bcc(111) surface were consistent with scattering or spectroscopic experiments. We expect that our analyses here can also be subjected to experimental confirmation via similar spectroscopic experimental techniques on Fe-bcc(211) surfaces.

4. CONCLUSIONS

We examined 49 distinct elements as dopants for the Febcc(211)R surface to seek an improved rate of NH₃ syntheses. Here, we used our previously proposed HHTCS strategy to reduce the effort needed to find the most promising dopants. Given the more complex character of the Fe-bcc(211)R with respect to the previously investigated Fe-bcc(111) surface, we had to correspondingly extend the HHTCS approach using multiple reference states to examine the possible dopant sites and their stability to be used in HHTCS screening criteria.

HHTCS predicts that of the 49, only Zr, Ru, and Co all increase the rate, with Co dramatically decreasing the overall free-energy barrier for catalytic NH₃ synthesis under industrial conditions.

We then carried out QM calculations to determine all steps in the synthesis reaction pathway for Fe-bcc(211)R, concluding that Co leads to a 0.19 eV decrease in the rate-determining step of N₂ dissociation. Using the DFT-predicted free-energy activation barriers in a kMC analysis, we predict that the Codoped Fe-bcc(211)R catalytic surface increases the TOF from 3.5 to 10.9 NH $_3$ /s per 2 × 2 cell at 673 K and increases the TOF from 682 to 2691 NH $_3$ /s per 2 × 2 cell at 773 K. This allows the total pressure to be decreased from 200 atm for pure Fe to 40 atm at T = 773 K for the Co-doped Fe-bcc(211)R surface compared to 200 atm at T = 773 K for the pure Fe-bcc(211)R surface, suggesting near-identical catalytic efficiency at lower pressures for the Co-doped Fe catalyst. The increase in cost of the catalyst due to the greater cost of cobalt should be offset by the relatively minor amount of Co needed for this doping scheme (only enough to dope the second layer) and the large increase in TOF with the connected possibility especially to decrease the operating pressure. Considering that Co doping of Fe-bcc(111) seems to increase the TOF in HB catalysis also for this different surface, ⁴⁸ Co is proposed as a strong candidate for improving the industrial HB process, possibly in multiple doping schemes in combination with other dopants.

Analysis of bonding on the undoped and doped surface indicates that the Co-doped surface increases the spin of Fe atoms in the resting state involved in the primary barrier, with weakened π -bonds and reoriented σ -bonds due to the doped Co atom in the $2N-2H-N_2(F)$ state, which leads to an alternate more stable bonding position. The finding that the Co dopant influences N2 bonding across an atomic layer in a nonadjacent position seems novel and indicates a possible role for these more distant doping positions for future computational work on reactions on surfaces. Both these phenomena contribute to decreasing the overall barrier compared to the pure Fe surface, demonstrating that metal spins can be used as quantitative descriptors of binding of adsorbates to magnetic transitionmetal surfaces. Our predictions on spin distributions and changes upon doping await experimental validation via scattering and Mössbauer or other spectroscopic experiments, while we trust that our kinetic results will trigger experimental catalytic testing.

ASSOCIATED CONTENT

Supporting Information

The Supporting Information is available free of charge at https://pubs.acs.org/doi/10.1021/acs.chemmater.0c02701.

Preferred positions of elements in the first and second layer for Fe-bcc(211)R; lowest-energy state for doping elements in Fe-bcc(211)R; convergence with respect to kMC steps for Co-doped and pure Fe-bcc(211)R surfaces; preferred positions of HHTCS elements; surface behavior of large elements; potential energy curves for hydrogenation transition states; potential energy curves for nitrogen dissociation transition states; and full reaction pathway for the undoped Fe-bcc(211)R surface (PDF)

Raw DFT data for HHTCS (XLSX)

Raw data for the reaction energy path of the HB process on the Co-doped Fe-bcc(211)R surface (XLSX)

AUTHOR INFORMATION

Corresponding Authors

Alessandro Fortunelli — Materials and Process Simulation Center (MSC), California Institute of Technology, Pasadena, California 91125, United States; CNR-ICCOM, Consiglio Nazionale delle Ricerche, ThC2-Lab, Pisa 56124, Italy; orcid.org/0000-0001-5337-4450;

Email: alessandro.fortunelli@cnr.it

William A. Goddard, III — Materials and Process Simulation Center (MSC), California Institute of Technology, Pasadena, California 91125, United States; orcid.org/0000-0003-0097-5716; Email: wag@caltech.edu

Qi An — Department of Chemical and Materials Engineering, University of Nevada—Reno, Reno, Nevada 89557, United States; orcid.org/0000-0003-4838-6232; Email: qia@ unr.edu

Author

Jon Fuller – Department of Chemical and Materials Engineering, University of Nevada–Reno, Reno, Nevada 89557, United States

Complete contact information is available at: https://pubs.acs.org/10.1021/acs.chemmater.0c02701

Notes

The authors declare no competing financial interest.

ACKNOWLEDGMENTS

J.F. was supported by DOE-NEUP under grant no. DE-NE0008889. A.F. gratefully acknowledges the contribution of the International Research Network IRN on Nanoalloys (CNRS). A.F. and WAG received support from NSF (CBET-1805022).

REFERENCES

- (1) U.S. Geological Survey. Mineral Commodity Summaries, 2018.
- (2) Aika, K.; Neilsen, A. Ammonia: Catalysis and Manufacture; Springer-Verlag: New York, NY, 1995.
- (3) Jennings, J. R. Catalytic Ammonia Synthesis: Fundamentals and Practice; Springer Science & Business Media: Berlin, Germany, 2013.
- (4) King, D. A.; Woodruff, D. P. The Chemical Physics of Solid Surfaces and Heterogeneous Catalysis; Elsevier Scientific Pub. Co.: New York, NY, 1981.
- (Ś) Ertl, G.; Knözinger, H.; Weitkamp, J. Handbook of Heterogeneous Catalysis; VCH: Weinheim, Germany, 1997.
- (6) Schlögl, R. Catalytic Synthesis of Ammonia—A "Never-Ending Story"? Angew. Chem., Int. Ed. 2003, 42, 2004–2008.
- (7) Ertl, G. Primary Steps in Catalytic Synthesis of Ammonia. J. Vac. Sci. Technol., A 1983, 1, 1247–1253.
- (8) Somorjai, G. A.; Materer, N. Surface Structures in Ammonia Synthesis. *Top. Catal.* **1994**, *1*, 215–231.
- (9) Hagen, S.; Barfod, R.; Fehrmann, R.; Jacobsen, C. J. H.; Teunissen, H. T.; Ståhl, K.; Chorkendorff, I. New Efficient Catalyst for Ammonia Synthesis: Barium-promoted Cobalt on Carbon. *Chem. Commun.* **2002**, 1206—1207.
- (10) Mortensen, J. J.; Hansen, L. B.; Hammer, B.; Nørskov, J. K. Nitrogen Adsorption and Dissociation on Fe(111). *J. Catal.* **1999**, *182*, 479–488.
- (11) Qian, J.; An, Q.; Fortunelli, A.; Nielsen, R. J.; Goddard, W. A. Reaction Mechanism and Kinetics for Ammonia Synthesis on the Fe(111) Surface. J. Am. Chem. Soc. 2018, 140, 6288–6297.
- (12) Fuller, J.; Fortunelli, A.; Goddard III, W. A.; An, Q. Reaction Mechanism and Kinetics for Ammonia Synthesis on the Fe(211) Reconstructed Surface. *Phys. Chem. Chem. Phys.* **2019**, 21, 11444–11454.

- (13) Yiokari, C. G.; Pitselis, G. E.; Polydoros, D. G.; Katsaounis, A. D.; Vayenas, C. G. High-Pressure Electrochemical Promotion of Ammonia Synthesis over an Industrial Iron Catalyst. *J. Phys. Chem. A* **2000**, *104*, 10600–10602.
- (14) Zhou, F.; Azofra, L. M.; Ali, M.; Kar, M.; Simonov, A. N.; McDonnell-Worth, C.; Sun, C.; Zhang, X.; MacFarlane, D. R. Electro-Synthesis of Ammonia from Nitrogen at Ambient Temperature and Pressure in Ionic Liquids. *Energy Environ. Sci.* **2017**, *10*, 2516–2520.
- (15) Furuya, N.; Yoshiba, H. Electroreduction of Nitrogen to Ammonia on Gas-Diffusion Electrodes Loaded with Inorganic Catalyst. *J. Electroanal. Chem. Interfacial Electrochem.* **1990**, 291, 269–272.
- (16) Guo, C.; Ran, J.; Vasileff, A.; Qiao, S.-Z. Rational design of electrocatalysts and photo(electro)catalysts for nitrogen reduction to ammonia (NH₃) under ambient conditions. *Energy Environ. Sci.* **2018**, 11, 45–56.
- (17) Swearer, D. F.; Knowles, N. R.; Everitt, H. O.; Halas, N. J. Light-Driven Chemical Looping for Ammonia Synthesis. *ACS Energy Lett.* **2019**, *4*, 1505–1512.
- (18) Kitano, M.; Kanbara, S.; Inoue, Y.; Kuganathan, N.; Sushko, P. V.; Yokoyama, T.; Hara, M.; Hosono, H. Electride Support Boosts Nitrogen Dissociation over Ruthenium Catalyst and Shifts the Bottleneck in Ammonia Synthesis. *Nat. Commun.* **2015**, *6*, 6731.
- (19) An, Q.; Shen, Y.; Fortunelli, A.; Goddard, W. A. QM-Mechanism-Based Hierarchical High-Throughput in Silico Screening Catalyst Design for Ammonia Synthesis. *J. Am. Chem. Soc.* **2018**, *140*, 17702–17710.
- (20) McDonald, M.; Fuller, J.; Fortunelli, A.; Goddard, W. A.; An, Q. Highly Efficient Ni-Doped Iron Catalyst for Ammonia Synthesis from Quantum-Mechanics-Based Hierarchical High-Throughput Catalyst Screening. *J. Phys. Chem. C* **2019**, *123*, 17375–17383.
- (21) An, Q.; Mcdonald, M.; Fortunelli, A.; Goddard, W. A. Si-Doped Fe Catalyst for Ammonia Synthesis at Dramatically Decreased Pressures and Temperatures. J. Am. Chem. Soc. 2020, 142, 8223–8232.
- (22) Kresse, G.; Hafner, J. Ab Initio Molecular-Dynamics Simulation of the Liquid-Metal—Amorphous-Semiconductor Transition in Germanium. *Phys. Rev. B: Condens. Matter Mater. Phys.* **1994**, 49, 14251—14269.
- (23) Kresse, G.; Furthmüller, J. Efficiency of Ab-initio Total Energy Calculations for Metals and Semiconductors using a Plane-Wave Basis set. Comput. Mater. Sci. 1996, 6, 15–50.
- (24) Kresse, G.; Furthmüller, J. Efficient Iterative Schemes for Ab Initio Total-Energy Calculations using a Plane-Wave Basis Set. *Phys. Rev. B: Condens. Matter Mater. Phys.* 1996, 54, 11169–11186.
- (25) Perdew, J. P.; Burke, K.; Érnzerhof, M. Generalized Gradient Approximation Made Simple. *Phys. Rev. Lett.* **1996**, *77*, 3865–3868.
- (26) Ernzerhof, M.; Perdew, J. P.; Burke, K. Coupling-Constant Dependence of Atomization Energies. *Int. J. Quantum Chem.* **1997**, *64*, 285–295.
- (27) Johnson, E. R.; Becke, A. D. A Post-Hartree-Fock Model of Intermolecular Interactions: Inclusion of Higher-order Corrections. *J. Chem. Phys.* **2006**, *124*, 174104.
- (28) Henkelman, G.; Uberuaga, B. P.; Jónsson, H. A Climbing Image Nudged Elastic Band Method for Finding Saddle Points and Minimum Energy Paths. J. Chem. Phys. **2000**, 113, 9901–9904.
- (29) Henkelman, G.; Jónsson, H. Improved Tangent Estimate in the Nudged Elastic Band Method for Finding Minimum Energy Paths and Saddle Points. *J. Chem. Phys.* **2000**, *113*, 9978–9985.
- (30) Kampshoff, E.; Waelchli, N.; Menck, A.; Kern, K. Hydrogen-Induced Missing-Row Reconstructions of Pd(110) Studied by Scanning Tunneling Microscopy. *Surf. Sci.* **1996**, *360*, 55–60.
- (31) Wang, T.; Wang, S.; Luo, Q.; Li, Y.-W.; Wang, J.; Beller, M.; Jiao, H. Hydrogen Adsorption Structures and Energetics on Iron Surfaces at High Coverage. *J. Phys. Chem. C* **2014**, *118*, 4181–4188.
- (32) Wang, T.; Tian, X.; Yang, Y.; Li, Y.-W.; Wang, J.; Beller, M.; Jiao, H. Coverage-Dependent N2 Adsorption and Its Modification of Iron Surfaces Structures. *J. Phys. Chem. C* **2016**, *120*, 2846–2854.
- (33) Zhang, J.-M.; Ma, F.; Xu, K.-W. Calculation of the Surface Energy of bcc Metals by using the Modified Embedded-Atom Method. *Surf. Interface Anal.* **2003**, 35, 662–666.

- (34) Yu, J.; Lin, X.; Wang, J.; Chen, J.; Huang, W. First-Principles Study of the Relaxation and Energy of bcc-Fe, fcc-Fe and AISI-304 Stainless Steel Surfaces. *Appl. Surf. Sci.* **2009**, 255, 9032–9039.
- (35) Baxter, R. J.; Hu, P. Insight into Why the Langmuir-Hinshelwood Mechanism is Generally Preferred. *J. Chem. Phys.* **2002**, *116*, 4379–4381
- (36) McKay, H. L.; Jenkins, S. J.; Wales, D. J. Theory of NHx ± H Reactions on Fe{211}. *J. Phys. Chem. C* **2009**, *113*, 15274–15287.
- (37) Gillespie, D. T. A General Method for Numerically Simulating the Stochastic Time Evolution of Coupled Chemical Reactions. *J. Comput. Phys.* **1976**, 22, 403–434.
- (38) Stamatakis, M. Kinetic Modelling of Heterogeneous Catalytic Systems. *J. Phys.: Condens. Matter* **2014**, 27, 013001.
- (39) Vineyard, G. H. Frequency Factors and Isotope Effects in Solid State Rate Processes. J. Phys. Chem. Solids 1957, 3, 121–127.
- (40) Logadóttir, A.; Nørskov, J. K. Ammonia synthesis over a Ru(0001) surface studied by density functional calculations. *J. Catal.* **2003**, 220, 273–279.
- (41) Honkala, K.; Hellman, A.; Remediakis, N.; Logadottir, A.; Carlsson, A.; Dahl, S.; Christensen, C. H.; Norskov, J. K. Ammonia Synthesis from First-Principles Calculations. *Science* **2005**, 307, 555–558
- (42) Gouveia, J. D.; Morales-García, Á.; Viñes, F.; Gomes, J. R. B.; Illas, F. Facile Heterogeneously Catalyzed Nitrogen Fixation by MXenes. ACS Catal. 2020, 10, 5049–5056.
- (43) Abghoui, Y.; Garden, A. L.; Hlynsson, V. F.; Bjorgvinsdottir, S.; Olafsdottir, H.; Skulason, E. Enabling electrochemical reduction of nitrogen to ammonia at ambient conditions through rational catalyst design. *Phys. Chem. Chem. Phys.* **2015**, *17*, 4904–4918.
- (44) Wang, X.; Peng, X.; Chen, W.; Liu, G.; Zheng, A.; Zheng, L.; Ni, J.; Au, C.-T.; Jiang, L. Insight into dynamic and steady-state active sites for nitrogen activation to ammonia by cobalt-based catalyst. *Nat. Commun.* **2020**, *11*, 653.
- (45) Zeinalipour-Yazdi, C. D.; Hargreaves, J. S. J.; Catlow, C. R. A. Low-T Mechanisms of Ammonia Synthesis on Co₃Mo₃N. *J. Phys. Chem. C* **2018**, 122, 6078–6082.
- (46) Niemantsverdriet, J.; van Kaam, J. A. C.; Flipse, C. F. J.; van der Kraan, A. M. Mössbauer and X-ray Photoelectron Spectroscopic Evidence for the Structure of Supported Bimetallic Catalysts: FeRu, FeRh, FePd, Felr, and FePt on SiO₂. *J. Catal.* **1985**, *96*, 58–71.
- (47) Whitman, L. J.; Bartosch, C. E.; Ho, W. A New Mechanism for K Promotion of Surface Reactions: N_2 on K-precovered Fe(111). *J. Chem. Phys.* **1986**, *85*, 3688.
- (48) Qian, J.; Fortunelli, A.; Goddard, W. A. Effect of Co doping on mechanism and kinetics of ammonia synthesis on Fe(111) surface. *J. Catal.* **2019**, 370, 364–371.